City, University of London Institutional Repository

Formation number of confined vortex rings
(to appear in *Physical Review Fluids, 2018*)

I. Danaila* and F. Luddens
Laboratoire de Mathématiques Raphaël Salem,
Université de Rouen Normandie,
76801 Saint-Étienne-du-Rouvray, France

F. Kaplanski, A. Papoutsakis, and S.S. Sazhin
Advanced Engineering Centre, Sir Harry Ricardo Laboratories,
School of Computing, Engineering and Mathematics,
University of Brighton, Brighton BN2 4GJ, U.K.
(Dated: September 20, 2018)

This paper investigates the formation number of vortex rings generated by a piston-cylinder mechanism in a confined tube. We use Direct Numerical Simulations (DNS) of axisymmetric confined vortex rings to study the influence of different parameters on the separation (or pinch-off) of the vortex ring from the trailing jet. It is shown that the structure of the vortex ring at pinch-off depends on the type of injection program (pulse dominated by either positive or negative acceleration ramps) and the confinement ratio D_w/D, where D_w is the inner diameter of the tube and D the diameter of the cylinder). For low confinement ratios ($D_w/D \leq 2$), a vortex of opposite sign generated at the lateral wall strongly interacts with the vortex ring and the pinch-off is not clearly observed. The pinch-off is observed and analysed for confinement ratios $D_w/D \geq 2.5$. DNS data are used to estimate the value of the formation time, which is the time necessary for the vortex generator to inject the same amount of circulation as carried by the detached vortex ring. The confined vortex ring at pinch-off is described by the model suggested by Danaila, Kaplanski and Sazhin [A model for confined vortex rings with elliptical core vorticity distribution, Journal of Fluid Mechanics, **811**:67-94, 2017]. This model allows us to take into account the influence of the lateral wall and the elliptical shape of the vortex core. The value of the formation time is predicted using this model and the slug-flow model.

* Corresponding author: ionut.danaila@univ-rouen.fr

I. INTRODUCTION

Laminar vortex rings are usually produced in the laboratory by pushing a column of fluid of length L through a long cylinder of diameter D using a piston moving with a time-dependent velocity $U_p(t)$. For large piston stroke ratios ($L/D > 2$), Gharib et al. [1] observed that the resulting flow consisted of a leading vortex ring followed by a trailing jet. The vorticity field of the leading vortex ring was disconnected from the trailing jet at a critical time instant (pinch-off time). When measuring the total circulation of the pinched-off vortex ring it was shown that it represents only a fraction of the circulation produced at the tip of the cylinder by the motion of the piston. The critical time at which the vortex generator produces the amount of circulation absorbed by the vortex ring was called the formation time (t_f) and the corresponding stroke ratio $F = (L/D)(t_f) = (1/D) \int_0^{t_f} U_p(\tau) d\tau$, the formation number (see Krueger and Gharib [2]). Note that for a constant piston velocity $U_p(t) = U_0$, the formation number can be expressed as $F = (L/D)_f = \tilde{t}_f$, where $\tilde{t}_f = t_f/(D/U_0)$ is the non-dimensional formation time. For long injection programs with $L/D > F$, the circulation generated by the piston after the formation time is engulfed solely in the trailing jet. Thus, the formation number describes the optimal scale for generated vortex rings and is related to the Kelvin-Benjamin maximization principle for the formation of vortex rings [3]. As a consequence, optimal pulsing conditions based on this result were investigated for various practical systems, including cardiac flows [4], the pulsatile propulsion of aquatic creatures [5, 6], synthetic jet actuators and propulsion devices [7, 8].

The investigation of the universality of the formation number resulted in a large body of literature. The value of the formation number F was found to be in the range 3.6 to 4.5 for laminar vortex rings [1]. Subsequent studies showed that this value depends on a number of factors, including the velocity profile at the vortex generator exit [9], the diameter of the vortex generator [10], the surrounding co-flow [11] or counterflow [12], and the piston velocity program [2, 13]. Values for F in the range 1 to 8 were reported. The concept of the formation number was extended to more complex vortex ring flows, such as buoyant plumes [14], negatively buoyant jets [15], and turbulent vortex rings [8], but it has not yet been investigated for confined vortex rings.

The primary focus of this study is on the existence and the value of the formation number for confined laminar vortex rings. The properties of vortex rings in unbounded domains have been studied for over a century both theoretically and experimentally (see the reviews by Shariff and Leonard [16], Lim and Nickels [17], and Fukumoto [18]). Surprisingly though, the investigation of confined vortex ring flows is far less developed despite its obvious relevance for practical applications, ranging from vortex ring-like structures in gasoline engines [19] to transient flow fields in biological complex systems [4]. The recent experimental study by Stewart et al. [20] demonstrated important differences between the evolution of a vortex ring confined in a tube and its evolution in an unbounded domain, but the low stroke ratios used for these experiments did not allow the authors to investigate the problem of the existence of the formation number for such flows. In the present study, Direct Numerical Simulations (DNS) will be used to establish the pinch-off and formation number of confined laminar vortex rings (Section II).

In Section III, we will use the approach suggested by Shusser and Gharib [21] to predict the value of the formation number. Assuming that the pinch-off occurs when the translational velocity of the vortex ring exceeds the velocity of the trailing jet, we match non-dimensional hydrodynamic integral quantities (energy and/or circulation) generated by the vortex generator (cylinder), with those measured for the pinched-off vortex ring. Numerous previous studies [3, 7, 21–24] used the classical [16, 17] or the corrected [23, 25] slug-flow model to characterise the vortex generator and the Norbury-Fraenkel [26] inviscid vortex ring model for the pinched-off vortex ring. The Norbury-Fraenkel model has severe limitations in describing confined vortex rings. For example, the vorticity distribution in the vortex core is assumed to be linear, i.e. proportional to the distance to the axis of symmetry (as in Hill's spherical vortex model), which is far from the quasi-Gaussian distribution observed for unconfined [27, 28] or confined vortex rings [20, 29, 30]. The model recently suggested by Danaila et al. [30] to describe confined and viscous vortex rings with an elliptical vortex core is used in this study. It will be shown that taking into account the ellipticity of the vortex ring core and the influence of the lateral wall leads to a more accurate prediction of the formation number.

II. DIRECT NUMERICAL SIMULATIONS (DNS) OF A VISCOUS AXISYMMETRIC VORTEX RING IN A TUBE

In this section, we use the results of Direct Numerical Simulation of axisymmetric incompressible flows to investigate some of the features of confined vortex rings at pinch-off. The numerical code for solving the incompressible Navier-Stokes equations in cylindrical coordinates was developed by Danaila and Helie [31] (see also [29, 32]). The incompressible Navier-Stokes equations written in cylindrical coordinates (r, θ, x) were solved using the numerical method suggested by Rai and Moin [33] and modified by Verzicco and Orlandi [34]. The method is described in detail by Orlandi [35] (see also [36]). The equations were written in primitive variables $(r v_r, v_\theta, v_x)$ and solved on a staggered grid to avoid the problem of singularities at the axis $r = 0$. Second order finite differences were used for the spatial

discretisation. For time advancement, the fractional-step method described by Kim and Moin [37] was used. This method is based on a combination of a low-storage third-order Runge–Kutta scheme for convective terms and the semi-implicit Crank–Nicolson scheme for viscous terms. At each substep of the Runge–Kutta scheme, the momentum equations were solved by the approximate factorisation technique (see Kim and Moin [37]) and the Poisson equation was solved for the pressure correction. The Poisson solver uses a fast Fourier transformation following the azimuthal direction θ, and an effective cyclic reduction method (Fishpack subroutines) for solving the remaining two-dimensional system following the r and x directions. The method is globally second order accurate in space and time.

A. Physical and numerical parameters

The computational configuration is sketched in Figure 1a). We consider the case of laminar vortex rings produced by pushing a column of fluid using a piston-cylinder mechanism [1] through a long pipe of diameter $D = 2R$. Let us introduce $D_0 = 2R_0$ as the vortex ring diameter and $D_w = 2R_w$ as the diameter of the tube. In what follows, all parameters are normalised using D as the length-scale and the maximum piston velocity U_0 as the velocity scale. The main physical parameter of the flow is the Reynolds number based on the pipe diameter:

$$Re_{\mathrm{D}} = \frac{U_0\,D}{\nu}, \tag{1}$$

where ν is the fluid kinematic viscosity. Using the time scale $t_0 = D/U_0$, the non-dimensional time in simulations is defined as:

$$\tau = \frac{tU_0}{D} = Re_{\mathrm{D}}\left(\frac{R_0}{D}\right)^2 t^*, \quad t^* = \frac{\nu t}{R_0^2}, \tag{2}$$

where t^* denotes the time scale related to the vortex ring evolution.
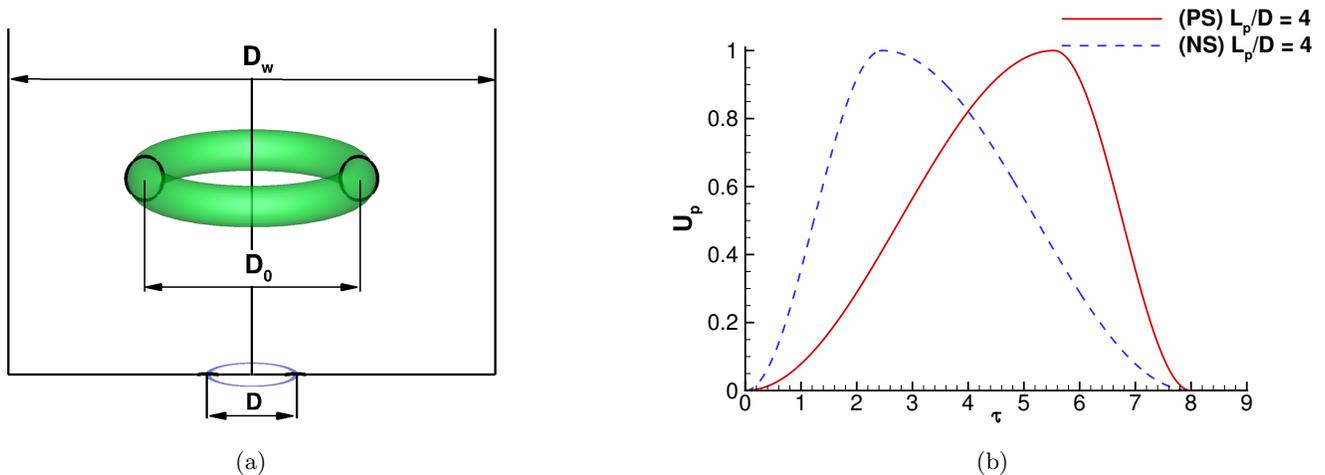
FIG. 1. (a) Schematic of a vortex ring in a tube. (b) Time evolution of the piston velocity $U_p(\tau)$: PS (positive sloping) ramp and NS (negative sloping) ramp programs.

The piston/cylinder generator was not simulated in this study. The vortex ring was generated numerically by prescribing an appropriate axial velocity profile at the outlet section of the cylinder, corresponding to the inlet section of the computational domain. We used a specified discharge velocity (SDV) [32]

$$U_{\mathrm{SDV}}(r,\tau) = U_0\,U_p(\tau)\,U_b(r,\tau), \tag{3}$$

where $U_p(\tau)$ is the piston velocity program (normalised by its maximum value U_0). To reproduce the impulsive injection program used in recent experiments with confined vortex rings by Stewart et al. [20], we considered a model for $U_p(\tau)$ similar to that suggested by Zhao et al. [38]:

$$U_p(\tau) = \begin{cases} \dfrac{1}{2}\left[1 - \cos\left(\pi\dfrac{\tau}{\tau_1}\right)\right], & \tau \leq \tau_1 \\[2mm] \dfrac{1}{2}\left[1 + \cos\left(\pi\dfrac{\tau - \tau_1}{\tau_2 - \tau_1}\right)\right], & \tau_1 < \tau \leq \tau_2 \approx \tau_{\mathrm{off}}. \end{cases} \tag{4}$$

The main integral characteristics of the vortex generator can be approximately estimated by the so-called slug-model [16, 17]. This model assumes that at the exit plane of the vortex generator the flow is parallel to the axis and the rate of change of the circulation is determined by the vorticity flux across this plane. Thus, the stroke length (L_p), circulation (Γ_p), impulse (I_p) and kinetic energy (E_p) of the discharged fluid at the cylinder tip are calculated as:

$$L_p = \int_0^{\tau_{\text{off}}} U_p(\tau)d\tau, \quad \Gamma_p = \frac{1}{2}\int_0^{\tau_{\text{off}}} U_p^2(\tau)d\tau,$$

$$I_p = \frac{\pi D^2}{4}\int_0^{\tau_{\text{off}}} U_p^2(\tau)d\tau, \quad E_p = \frac{\pi D^2}{8}\int_0^{\tau_{\text{off}}} U_p^3(\tau)d\tau. \tag{5}$$

Program	τ_1	τ_2	L_p/D
PS	5.54	8	4
NS	2.46	8	4

TABLE I. Parameters τ_1, τ_2 of the injection program (4) and piston stroke ratios $L_p/D = \int_0^{\tau_{\text{off}}} U_p(\tau)d\tau$ corresponding to the PS (positive sloping) ramp and NS (negative sloping) ramp programs displayed in Figure 1 b).

The velocity programs displayed in Figure 1 b) are designed to obtain a piston stroke to diameter ratio $L_p/D = 4$. This is motivated by the fact that the pinch-off has been observed [1, 2] to occur at a stroke ratio of approximately 4. The corresponding values of time constants τ_1 and τ_2 are given in Table I. Recalling the results of the experimental study by Krueger and Gharib [2], we considered two types of injection programs: a pulse dominated by an acceleration phase (PS, positive sloping ramp) and a pulse with a velocity deceleration during most of the injection period (NS, negative sloping ramp). This allowed us to investigate the influence of the piston velocity program on the characteristics of the vortex ring and its trailing jet at the pinch-off. Note that in recent experiments of confined vortex rings by Stewart *et al.* [20], a PS-type program was used, but with a stroke ratio $L_p/D < 2$, which was too low to observe the pinch-off (no trailing jet was generated).

In the SDV model (3), $U_b(r,\tau)$ describes the radial dependence of the profile and takes the hyperbolic tangent form commonly used in jet-flow simulations [39]:

$$U_b(r,\tau) = \frac{1}{2}\left\{1 + \tanh\left[\frac{1}{4\Theta}\left(\frac{R}{r} - \frac{r}{R}\right)\right]\right\}, \tag{6}$$

where Θ is the non-dimensionalised vorticity thickness. As in most similar numerical simulations [38, 40], the parameters of the discharge velocity profile are assumed to be constant: $U_0 = 1$, $R = 0.5$ and $\Theta = 1/40$. In all simulations the Reynolds number was set to $Re_{\text{D}} = 3400$, as in the previous numerical studies of confined vortex rings [29].

The fluid inside the domain was initially ($\tau = 0$) at rest. We simulated the evolution of the vortex ring until $\tau = 24$. The length of the computational domain was taken as $L_d = 12$, which allowed us to avoid the vortex ring coming close to the downstream boundary, where we apply the convective boundary condition suggested by Orlanski [41], enforced by the global mass conservation procedure described by Ruith *et al.* [36]. At $r = R_w$ a non-slip wall boundary condition is imposed through a ghost-cell procedure. The singularity $r = 0$ did not require a special treatment, as the solver uses primitive variables ($q_r = rv_r$ and $q_x = v_x$) and a staggered grid. Only q_r was located at axis $r = 0$, where the following boundary conditions were used: $q_r = 0$ (per definition) and $\partial q_x/\partial r = 0$ (symmetry). At the inflow section ($x = 0$), the velocity was imposed: $q_x = U_{\text{SDV}}(r,\tau)$ (following the injection program (3)) and $q_r = 0$ (no radial velocity). After the injection stopped, a wall condition ($q_x = q_r = 0$) was imposed at the inflow section. The grid was uniform in both axial and radial directions with a refined grid size $\delta r = \delta x = 0.01$ which ensures grid convergence of the results. Tests with a stretched grid in the radial direction, such that at least 30 grid points were clustered within the vorticity layer at the inflow, showed identical results. The time step was set to $\delta\tau = 0.001$, which is below the admissible value imposed by the stability of the numerical scheme. Timestep refinement tests showed negligible differences in the results obtained for lower $\delta\tau$.

B. Numerical results

1. Pinch-off of the confined vortex ring

We first investigate the influence of the confinement parameter D_w/D on the vortex ring pinch-off. The piston stroke ratio parameter is fixed at $L_p/D = 4$. High confinements correspond to low D_w/D ratios, *i. e.* short distances between the centre of the vortex and the lateral wall. In the experimental study by Stewart *et al.* [20], considering a low stroke ratio ($L_p/D = 1.2$), the vortex ring was observed to be clearly formed (*i. e.* without significant influence of the lateral wall) only for confinements $D_w/D \geq 1.5$. This observation was confirmed by the numerical simulations of Danaila *et al.* [29]. Due to the larger stroke ratio in our study, we started our numerical investigation with a larger D_w/D confinement parameter. Figure 2 shows the early stage of the vortex ring formation for $D_w/D = 2$. After the injection stops ($\tau > \tau_{\text{off}} = 8$), the vortex ring continues to grow by engulfing vorticity from the trailing jet. The velocity induced by the vortex ring generates a vorticity layer at the lateral wall (Figure 2a) which rolls into a vortex with negative vorticity (Figure 2b) evolving on the top of a positive vorticity layer (see Figure 2c and the zoom in Figure 2d). The proximity of the primary vortex ring and the secondary vortex affects the separation of the vortex ring from its trailing jet. A clear vortex pinch-off process is difficult to observe in this case. Thus we considered larger confinement parameters ($D_w/D > 2$).
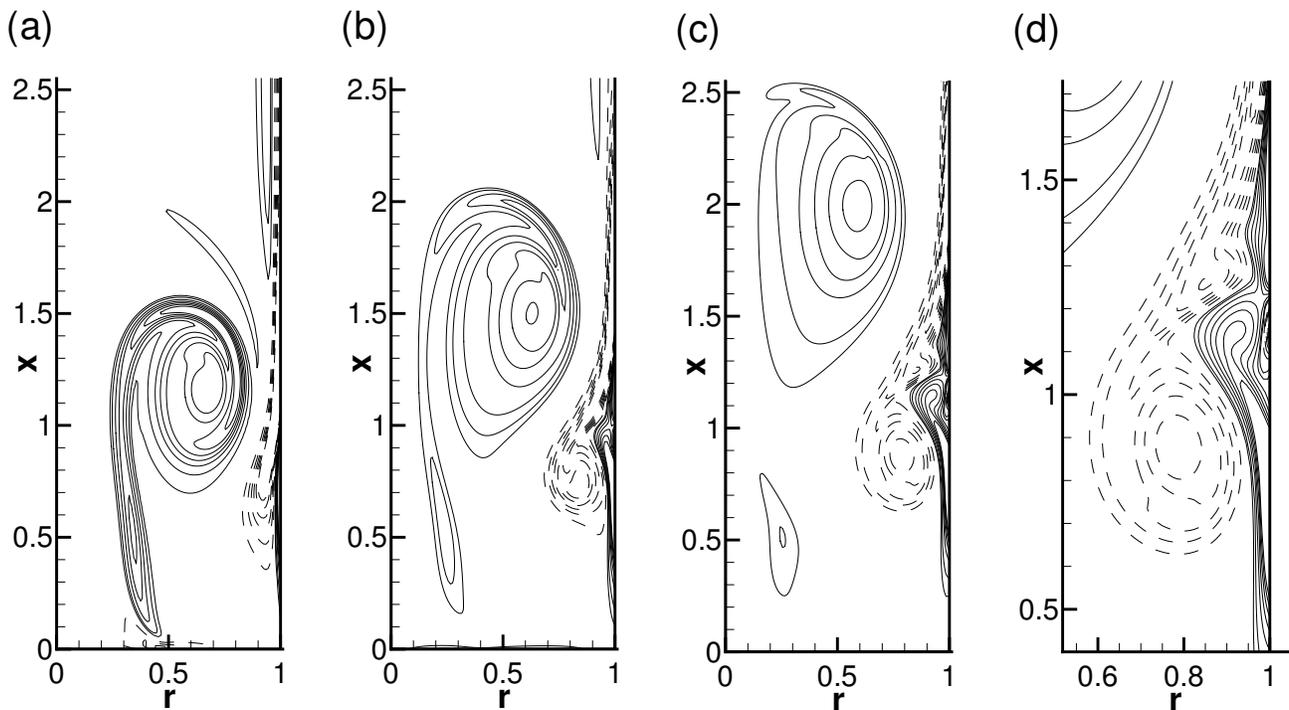

FIG. 2. Contours of vorticity ω at the early stage of formation of the vortex ring in a tube for a high confinement case ($D_w/D = 2$). Dashed curves show contours of negative vorticity. Values of ω from -6 to 6 with increments of 1 are shown. Plots (a, b, c) correspond to time instants $\tau = 8, 10, 12$. Plot (d) is a zoom of plot (c) showing the vortex structures generated at the lateral confinement wall. A PS injection program was used (see Table I).

Figure 3 shows clear evidence of the pinch-off process for confinement parameter $D_w/D = 2.5$. For this case, the vorticity layer at the wall is too weak to roll into a secondary vortex. After the injection is stopped, the pinch-off is observed for both PS (plots a, b, c) and NS (plots d, e, f) injection programs. The pinch-off occurs earlier for the NS injection program, when compared to the PS case (Figures 3b and 3e). This is explained by the higher acceleration of the piston motion in the NS program (Figure 1b). At $\tau_{\text{off}} = 8$ (Figures 3a and 3d) the vortex ring is formed farther downstream than in the PS case and has a higher peak vorticity. Hence, at pinch-off, the NS case displays a more significant trailing jet than the PS case (Figures 3c and 3e). A similar evolution was observed for unconfined vortex rings in the experimental study by Krueger and Gharib [2].
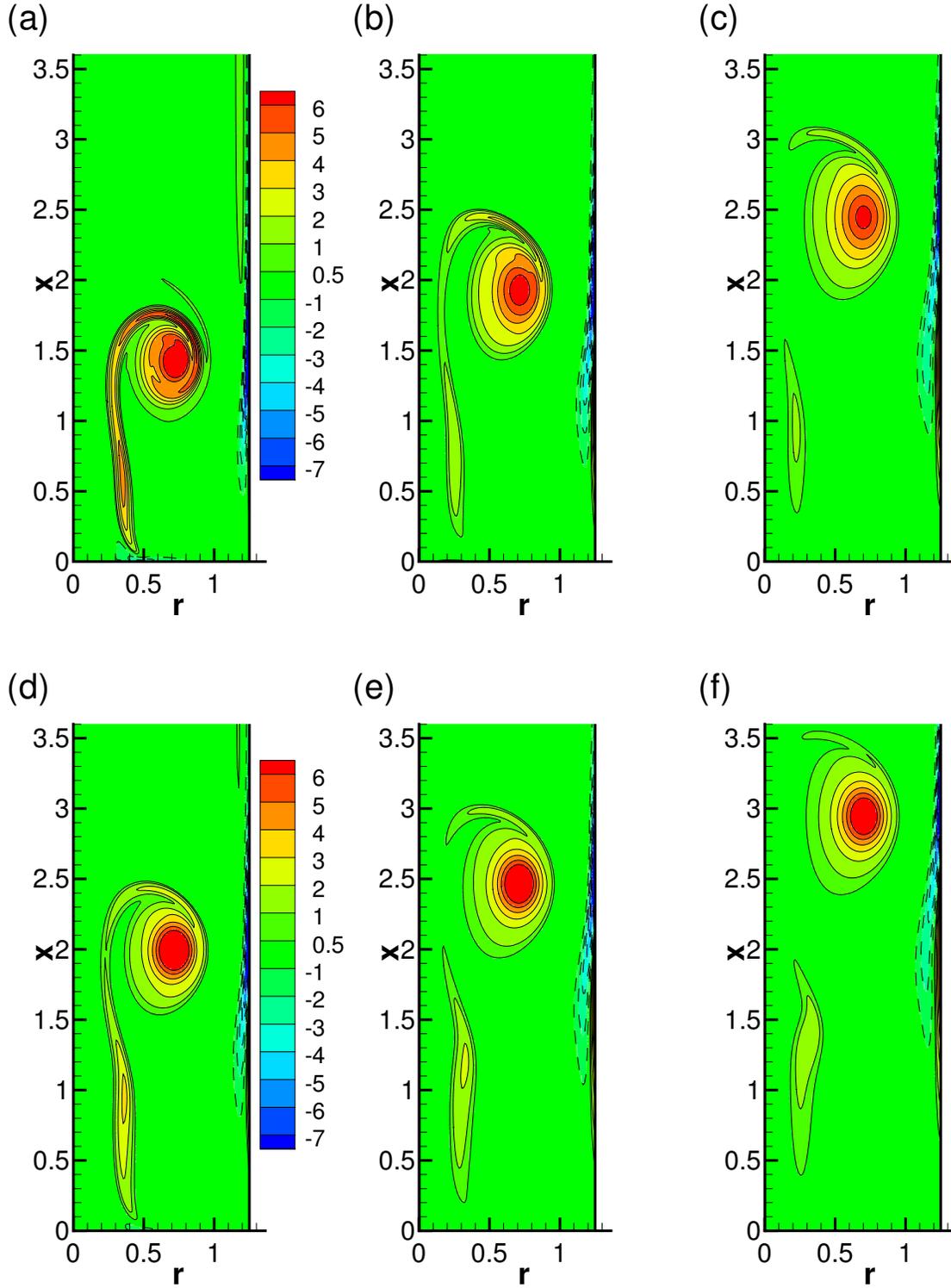
FIG. 3. Contours of vorticity ω at the early stage of formation of the vortex ring in a tube for a confinement parameter $(D_w/D = 2.5)$. Dashed curves show contours of negative vorticity. Plots (a, b, c) refer to the case of the PS injection program and (d, e, f) refer to the NS injection program (Figure 1b). Three time instants are illustrated for each case: $\tau = 8$ (a, d), $\tau = 10$ (b, e), $\tau = 12$ (c, f) (the injection was stopped at $\tau_{\text{off}} = 8$).

The difference between the PS and NS programs is also illustrated in Figure 4 which plots the time evolution of the parameters characterising the vortex ring strength and trajectory: the maximum value of the vorticity ω_{max} (Figure 4a) and the stream-wise position X_c (Figure 4b) of the vortex centre corresponding to the maximum vorticity. As expected, the value of ω_{max} for the vortex ring becomes larger and the ring travels faster when the confinement is reduced (D_w/D is increased). For all confinement ratios D_w/D under consideration, the NS injection program generates a vortex ring with a higher vorticity peak at its centre and higher translation velocity (measured as $dX_c/d\tau$). The rate of decrease of the maximum vorticity is higher for the NS case. We can conclude from Figures 3 and 4 that, for the same piston stroke ratio, the NS program generates a more intense (with a higher vorticity peak), more compact (less elongated) and faster (higher velocity) vortex ring than the one produced by the PS program. These characteristics (vorticity, velocity and geometrical parameters) will be taken into account in the next section for modelling the vortex rings at pinch-off.
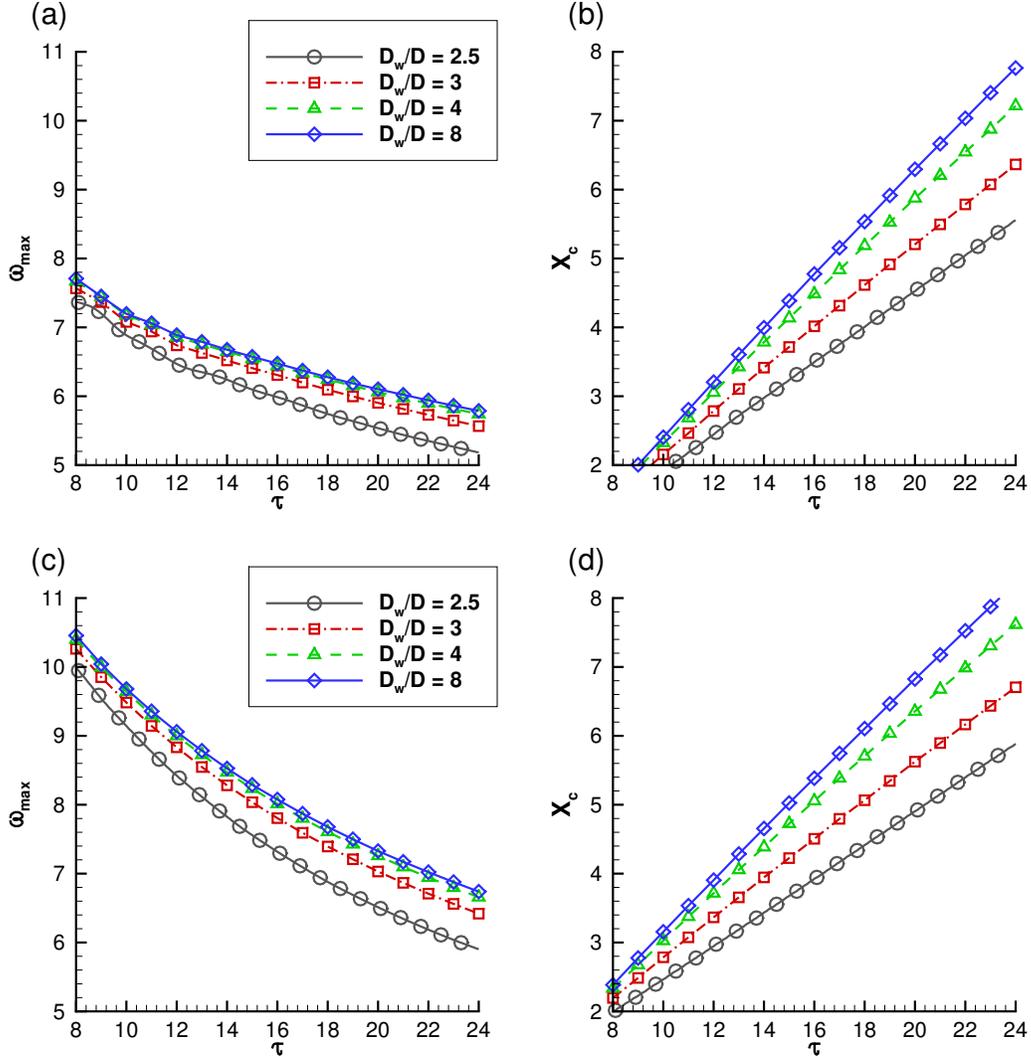
FIG. 4. Time evolution of the maximum vorticity ω_{max} and stream-wise position of the vorticity centre X_c corresponding to the maximum vorticity. PS injection program (a, b); NS injection program (c, d).

Also, Figure 4 shows that for $D_w/D \geq 4$, the lateral wall has no significant impact on the vortex ring evolution. The case $D_w/D = 8$ represents the asymptotic regime of an unconfined vortex ring. Note that, for lower piston stroke ratios ($L_p/D < 2$), the influence of the lateral wall was found to be negligible for $D_w/D \geq 3$ [20, 29]. This was expected, since a long injection time allows a longer and stronger interaction of the forming vortex ring with the lateral wall.

2. Formation time and formation number

At pinch-off, the vortex ring circulation Γ_{VR} represents only a part of the total circulation Γ_{inj} generated by the injection process. The time instant τ_f at which the vortex generator (piston/cylinder mechanism) produces exactly the same amount of circulation as the vortex ring at pinch-off was defined by Gharib *et al.* [1] as the *formation time* of the vortex ring. The corresponding piston displacement (L/D) is called the *formation number* and is denoted by F. To determine the value of the formation time for the confined vortex ring, the vortex ring has to be properly separated from the trailing jet. The presence of the lateral wall makes the separation of the vortex core rather delicate, since intense vorticity layers develop near this wall and at the inflow section after the injection stops. A special post-processing program, based on the free finite-element solver FreeFem++ [42, 43], was developed to properly separate the vortex ring core and compute flow integrals.

The velocity field obtained from the DNS simulations using second order finite-difference schemes is easily represented as a finite-element field by splitting each rectangular finite-difference cell into two triangles. The DNS values at the computational nodes are then used to represent the velocity field as a P_1 (piece-wise linear) function on the triangular mesh. This procedure avoids interpolations between the DNS finite-difference grid and the finite-element grid used for post-processing.

A general method used in numerical and experimental studies to separate a vortex ring consists of the following steps: the centre C of the vortex is first located as the point of maximum vorticity ω_{max}; the vortex core is then defined as the unique domain bounded by the vorticity contour $\omega/\omega_{max} = \omega_{cut}$ including the centre C. The cutoff level ω_{cut} is generally set based on trial and error. Threshold values have ranged from 2% and 5% in numerical studies [3, 9, 38, 44], to approximately 10% in experiments [45]. In our previous studies [29–31], the value $\omega_{cut} = 5\%$ proved optimal for identifying the vortex ring in the post-formation phase. In the present study, we defined the vorticity patch $\Omega_{0.05} = \{(r,x) \,|\, \omega(r,x)/\omega_{max} \geq 0.05\}$ and followed its evolution during both formation and post-formation phases. The level-set contour defining the boundary of $\Omega_{0.05}$ was accurately computed using P_1 finite-element interpolation. The vorticity layers near the inflow section ($x = 0$) and the lateral wall ($r = R_w$) were discarded before computing the level-set.

Before the pinch-off (formation phase), domain $\Omega_{0.05}$ is a simply connected open set, as illustrated for the PS injection program in Figures 5a ($\tau = 8$) and 5b ($\tau = 10$). After the pinch-off, domain $\Omega_{0.05}$ becomes disconnected, with two disjoint sets: $\Omega_{0.05} = \Omega_{\mathrm{VR}} \cup \Omega_{\mathrm{T}}$. The vortex ring domain Ω_{VR} contains the vortex centre C, while Ω_{T} represents the trailing jet near the inflow section (Figure 5c). Following the evolution of the vorticity patch $\Omega_{0.05}$ can thus be considered an effective practical method of detecting the pinch-off. Also, we show in Figure 5 the boundary of the vorticity patch $\Omega_{0.01}$, corresponding to $\omega_{cut} = 1\%$. Note that this cut-off level is too low to be used for the detection of the pinch-off, since $\Omega_{0.01}$ also includes the diffuse low vorticity region between the vortex ring and the trailing jet.
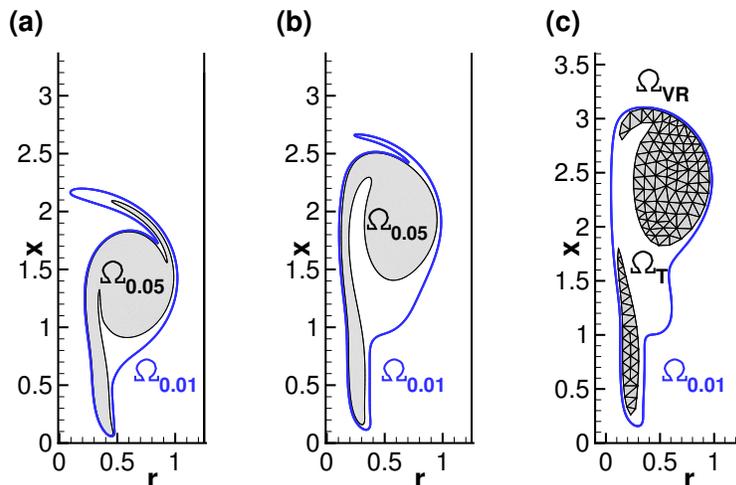
FIG. 5. Vorticity domain $\Omega_{0.05} = \{(r,x) \,|\, \omega(r,x)/\omega_{max} \geq 0.05\}$ (grey patches) used to compute integral quantities for the case of the PS injection program. Plots (a, b, c) refer to time instants $\tau = 8, 10, 12$. The corresponding vorticity fields are illustrated in Figure 3(a, b, c). The inside area of $\Omega_{0.05}$ is remeshed using triangular finite elements (a mesh using larger triangles than in the actual post-processing is shown for illustration in plot c). The border of the domain $\Omega_{0.01} = \{(r,x) \,|\, \omega(r,x)/\omega_{max} \geq 0.01\}$ is also shown (in blue).

Let Ω_* be a general vorticity patch used in the post-processing program. The domain Ω_* was remeshed with triangular finite elements to accurately represent the curved border of the domain (in Figure 5c very large triangles are used for illustration only). The DNS vorticity field was then interpolated to the new finite-element mesh, without any loss of accuracy. All operations (identifying the level-set, separating the simply connected sets, remeshing the domains inside level-set contours and, finally, interpolation of DNS data) were performed with basic functions available in FreeFem++. The finite-element representation of vorticity patches allowed us to use high (6th to 10th) order quadrature rules to compute the integral characteristics: circulation (Γ), hydrodynamic impulse (I) and energy (E):

$$\Gamma_* = \int_{\Omega_*} \omega \, dr dz, \; I_* = \pi \int_{\Omega_*} \omega r^2 dr dz, \; E_* = \pi \int_{\Omega_*} \omega \Psi dr dz. \tag{7}$$

The Stokes stream function Ψ is obtained by numerically solving the partial differential equation

$$\mathcal{L}\Psi = \omega \quad \text{in } \Omega_*, \quad \text{with} \quad \mathcal{L} := -\frac{\partial}{\partial r}\left(\frac{1}{r}\frac{\partial}{\partial r}\right) - \frac{\partial}{\partial x}\left(\frac{1}{r}\frac{\partial}{\partial x}\right), \tag{8}$$

and Dirichlet boundary conditions derived from the velocity field. Solving (8) with finite elements in FreeFem++ is very simple and takes only 5 lines of code, since $\mathcal{L}$ is a linear, self-adjoint elliptic operator.

Figure 6 shows the time evolution of circulation Γ_*, computed using this method, for $\Omega_* = \Omega_{0.05}$, $\Omega_{0.01}$ and Ω_{VR}. During the injection phase ($\tau \leq \tau_{off}$), the circulation increases rapidly and attains its maximum. For the formation phase, the values of $\Gamma_{0.01}$ and $\Gamma_{0.05}$ are very close (the maximum difference between them is 6%). This is expected as the vorticity during the injection is concentrated within a very thin layer (see Figures 3a and 3d) and the vorticity patch $\Omega_{0.01}$ differs from $\Omega_{0.05}$ by a small region of low vorticity (see Figure 5a). We assume that the circulation of the injection phase is represented by $\Gamma_{inj} = \Gamma_{0.05}$. This assumption is valid for $\tau \leq \tau_{off}$. After the pinch-off, it is possible to compute the circulation of the vortex ring Γ_{VR} and the circulation of the trailing jet Γ_T, using patches Ω_{VR} and Ω_T shown in Figure 5c. Since $\Omega_{0.05} = \Omega_{VR} \cup \Omega_T$, it follows from (7) that $\Gamma_{0.05} = \Gamma_{VR} + \Gamma_T$ after the pinch-off. Figure 6 shows that Γ_{VR} and $\Gamma_{0.01}$ are almost constant during the post-formation phase, while the circulation of the trailing jet ($\Gamma_{0.05} - \Gamma_{VR}$) decreases very quickly with τ. This observation and the corresponding increase of the difference ($\Gamma_{0.01} - \Gamma_{0.05}$) with τ, imply that the low vorticity region connecting the vortex ring to its tail rapidly spreads by viscous diffusion (see Figures 5b and 5c).
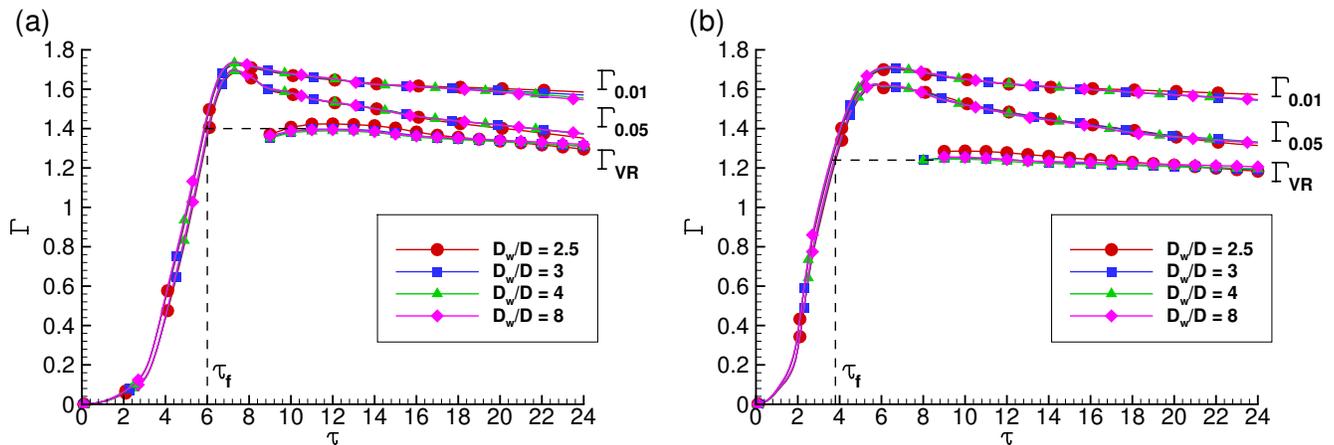

FIG. 6. Time evolution of circulation Γ_* computed from (7) for three vorticity patches ($\Omega_* = \Omega_{0.05}$, $\Omega_{0.01}$ and Ω_{VR}). The vortex ring circulation Γ_{VR} was computed only after the pinch-off. PS injection program (a) and NS injection program (b) were used.

The NS injection program generates the flow with the steepest increase in total circulation, but maximum values of the flow circulation are similar for NS ($\Gamma_{inj}^{max} = 1.63$) and PS ($\Gamma_{inj}^{max} = 1.70$) programs. Table II presents the parameters of the vortex ring at pinch-off, which is considered to occur at the time instant corresponding to the maximum value of the vortex ring circulation Γ_{VR} observed during the post-formation phase. The formation time τ_f is inferred from Figure 6 as the physical time necessary for the vortex generator to produce the circulation engulfed by the vortex ring at pinch-off, i. e. $\Gamma_{inj}(\tau_f) = \Gamma_{VR}$ (see the dashed curves in Figure 6). The piston displacement corresponds to the formation time $F = (L/D)_f = \int_0^{\tau_f} U_p(\tau) d\tau$.

	D_w/D	Γ_{VR}	τ_f	$F = (L/D)_f$	E^*_{VR}
PS	2.5	1.42	6.1	3.31	0.23
PS	3	1.39	6.0	3.22	0.26
PS	4	1.39	6.0	3.22	0.29
PS	8	1.39	6.0	3.22	0.31

	D_w/D	Γ_{VR}	τ_f	$F = (L/D)_f$	E^*_{VR}
NS	2.5	1.28	3.9	2.60	0.26
NS	3	1.24	3.8	2.51	0.31
NS	4	1.24	3.8	2.51	0.34
NS	8	1.25	3.8	2.51	0.35

TABLE II. Parameters of the vortex ring at pinch-off (see Figure 6): vortex ring circulation Γ_{VR}, formation time τ_f, formation number F (*i.e.* the piston displacement $(L/D)_f$ at formation time), and non-dimensional energy $E^*_{\text{VR}} = E_{\text{VR}}/(I^{1/2}_{\text{VR}}\Gamma^{3/2}_{\text{VR}})$. The parameters are computed for time instants corresponding to the maximum value of the vortex ring circulation Γ_{VR}.

Figure 6 and Table II show that the confinement ratio D_w/D has little influence on the formation number F for $D_w/D \geq 3$. The formation number ranges from 3.22 to 3.31 for the PS program and from 2.51 to 2.60 for the NS injection program. These values are slightly lower, when compared to those obtained experimentally by Krueger and Gharib [2] for the unconfined vortex ring: $F = 3.3 - 4.4$ for the PS case and $F = 2.4 - 2.9$ for the NS case. Krueger and Gharib suggested that a shift of approximately of $(L/D = 1)$ should be applied to obtain a collapse between the values of the formation numbers for the PS and NS cases. This suggestion holds for our results, obtained for confined vortex rings, if a shift of $L/D = 0.7$ is applied. Note that, for an unconfined vortex ring, numerous studies [1, 2, 7, 9–12, 14, 21, 22] have suggested various ways to manipulate the injection process and thus obtain different values of the formation number, ranging from 1 to 4.5.
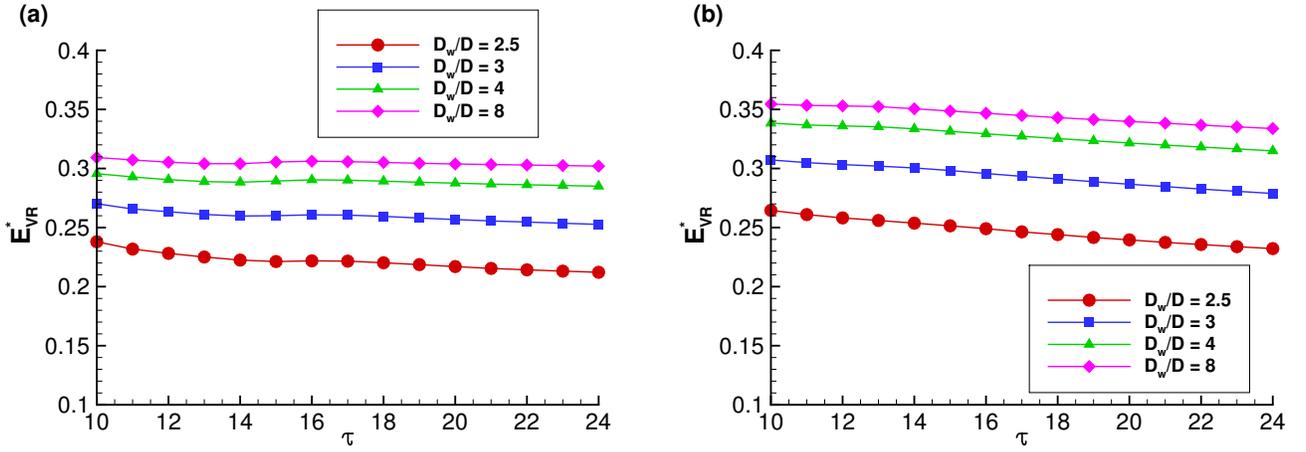

FIG. 7. Time evolution of the non-dimensional energy $E^*_{\text{VR}} = E_{\text{VR}}/(I^{1/2}_{\text{VR}}\Gamma^{3/2}_{\text{VR}})$ after pinch-off. PS (a) and NS (b) injection programs were used.

Also, Table II presents the values of the normalised energy $E^*_{\text{VR}} = E_{\text{VR}}/(I^{1/2}_{\text{VR}}\Gamma^{3/2}_{\text{VR}})$ at pinch-off. It has been shown [3, 22] that each vortex ring generator has a specific rate for feeding the flow with the kinetic energy, impulse, and circulation, resulting in specific values for E^*_{VR}. Figure 7 shows that E^*_{VR} is almost constant after the pinch-off and during the entire post-formation phase. This result will be useful in the next section which focuses on the theoretical prediction of the formation number. The time evolution of E^*_{VR} for the NS case decreases slightly and displays larger values than those obtained with the PS program for all confinement ratios. We can conclude that the confinement has little effect on the value of the non-dimensional energy E^*_{VR} of the pinched-off vortex for confinement ratios $D_w/D \geq 4$. The values of E^*_{VR} obtained for low confinements ($D_w/D = 8$) for both PS and NS injection programs are consistent with previous experimental and theoretical studies, suggesting that $E^*_{\text{VR}} \approx 0.3$ is a universal scale for unconfined vortex rings generated by a piston-cylinder mechanism [46]. For higher confinements, the value of E^*_{VR} is lower, suggesting that the interaction of the vortex ring with the lateral wall slows down the rate at which the vortex is fed with kinetic energy.

III.   THEORETICAL PREDICTION OF THE FORMATION NUMBER OF A CONFINED VORTEX RING

The idea behind most theoretical studies predicting the formation number of unconfined vortex rings is to match two models in terms of the non-dimensional hydrodynamic quantities (energy and/or circulation) characterising the vortex generator and the pinched-off vortex ring, respectively. For the former, the classical [16, 17] or corrected [23, 25] slug-flow model is used as a crude estimation, while the latter is based on a theoretical vortex ring model. The Norbury-Fraenkel model [26] for the inviscid vortex ring is commonly used to describe experimentally or numerically generated vortex rings and then estimate the formation number [3, 7, 21–24]. More realistic vortex ring models, taking into account viscous effects and the Gaussian distribution of the vorticity in the vortex core, were also used to predict the formation number of unconfined vortex rings [47, 48].

In the present work, we use the model recently suggested by Danaila *et al.* [30] to describe confined vortex rings with elliptically shaped vortex cores. We anticipate that taking into account the ellipticity of the core of the vortex ring will lead to a more accurate prediction of the formation number. We start by presenting the closed formulae of the vortex ring model and the fit between its parameters and DNS data. Finally we use the approach suggested by Shusser and Gharib [21], assuming that the pinch-off starts when the translational velocity of the vortex ring equals the velocity of the trailing jet.

A.   A model for confined vortex rings with elliptical cores

A theoretical model for a confined vortex ring was suggested by Brasseur [49, 50]. The stream function Ψ^w describing the flow generated by a vortex ring in a tube was presented as the sum of the stream function of an unbounded vortex ring Ψ and the wall-induced correction $(-\Psi^0)$:

$$\Psi^w(x,r) = \Psi(x,r) - \Psi^0(x,r). \tag{9}$$

Brasseur represented the unbounded vortex ring as a circular vortex filament (CVF) [51], with given initial circulation Γ_0 and radius R_0 (see Figure 1a). The correction Ψ^0 refers to a potential flow added to the CVF flow to satisfy the boundary condition at the wall, *i. e.* $\frac{1}{r}\frac{\partial \Psi}{\partial x} = \frac{1}{r}\frac{\partial \Psi^0}{\partial x}$, for $r = R_w$ (no flow through the tube wall). To derive the correction Ψ^0, the potential of the flow was expanded into a special series of harmonics, with the first harmonic being a point dipole and other terms the derivatives of that dipole [49]. Next, the point dipole was replaced with the Green function to Laplace's equation with Neumann boundary conditions, and used to derive a closed expression for the correction Ψ^0. An implicit assumption of Brasseur's approach was that the flow field far from the vortex core depends on its total circulation but not on the details of the vorticity distribution. Thus, Brasseur's model is completely described by the following expressions for vorticity and the Stokes stream function:

$$\omega_{\mathrm{CVF}} = \Gamma_0\,\delta(r-R_0)\delta(x-X_0), \tag{10}$$

$$\Psi_{\mathrm{CVF}} = \frac{\Gamma_0 R_0 r}{2} \int_0^\infty \exp(-x\mu) \mathrm{J}_1(R_0\mu)\mathrm{J}_1(r\mu)d\mu, \tag{11}$$

$$\Psi_{\mathrm{CVF}}^0 = \frac{\Gamma_0 R_0 r}{\pi} \int_0^\infty \frac{\mathrm{K}_1(\mu R_w)}{\mathrm{I}_1(\mu R_w)} \mathrm{I}_1(R_0\mu)\mathrm{I}_1(r\mu)\cos(x\mu)d\mu, \tag{12}$$

where δ is the Dirac delta function and X_0 the stream-wise position of the vortex centre. I_1 and K_1 are the modified Bessel functions of the first and second kind, respectively.

Danaila *et al.* [29] applied Brasseur's method using not the CVF but a more realistic vorticity distribution in the vortex ring core. Kaplanski and Rudi [47] derived an unconfined vortex ring model based on a linear first-order solution to the Navier-Stokes equation for an axisymmetric geometry and arbitrary times (see also [52]). The vorticity in this model (hereafter referred to as VRC, for *vortex rings with a circular core*) was predicted to be quasi-isotropic Gaussian, very close to that measured in experiments [27]:

$$\omega_{\mathrm{VRC}} = \frac{\Gamma_0}{R_0^2} \frac{\theta_c^3}{\sqrt{2\pi}} \exp\left(-\frac{(r_1^2 + x_1^2 + 1)\theta_c^2}{2}\right) \mathrm{I}_1\left(r_1\theta_c^2\right), \tag{13}$$

where

$$x_1 = \frac{x - X_0}{R_0}, \quad r_1 = \frac{r}{R_0}. \tag{14}$$

The model based on (13) uses a single geometric parameter θ_c, which makes it attractive for practical applications. Thus, the VRC class of vortex rings can be considered as the viscous analogue to Norbury's inviscid vortices. The main advantage of using this model is the better description of the vorticity distribution in the vortex core. Parameter θ_c depends on a viscous length-scale L_c:

$$\theta_c = \frac{R_0}{L_c}. \tag{15}$$

The original VRC model was based on the assumption of a time-dependent viscous scale: $L_c(t) = \sqrt{2\nu t}$, where ν is the fluid kinematic viscosity. The generalisation of this model for turbulent vortex rings was discussed in [53]. The model is valid not only in the limit of small Reynolds numbers $Re_{\mathrm{VR}} = \Gamma_0/\nu$, but also for large Re_{VR} at short times t (see Fukumoto and Kaplanski [48]). Using the vorticity distribution (13) and series expansions similar to that used in Brasseur's approach, Danaila *et al.* [29] derived closed analytical formulae for the stream function correction. Finally, the confined VRC model was described by the vorticity distribution (13) and the following two stream functions used in (9):

$$\Psi_{\mathrm{VRC}} = (\Gamma_0 R_0)\frac{r_1\theta_c}{4}\int_0^\infty \left[\exp(x_1\theta_c\mu)\mathrm{erfc}(\frac{\mu + x_1\theta_c}{\sqrt{2}}) + \exp(-x_1\theta_c\mu)\mathrm{erfc}(\frac{\mu - x_1\theta_c}{\sqrt{2}})\right]$$
$$\times \mathrm{J}_1(r_1\theta_c\mu)\mathrm{J}_1(\theta_c\mu)d\mu, \tag{16}$$

$$\Psi_{\mathrm{VRC}}^0 = (\Gamma_0 R_0)\frac{r_1}{\pi}\int_0^\infty \frac{\mathrm{K}_1(\mu/\varepsilon)}{\mathrm{I}_1(\mu/\varepsilon)}\mathrm{I}_1(\mu)\mathrm{I}_1(r_1\mu)\cos(x_1\mu)d\mu, \tag{17}$$

where J_1 is the Bessel function of the first kind and erfc the complementary error function. Note that the stream function correction (17) is identical to that found by Brasseur [49] for the circular vortex filament. The predictions of the confined VRC model were shown to be in agreement with available experimental data [20] and results of direct numerical simulations.

To further improve the VRC model for the confined vortex ring, Danaila *et al.* [30] took into account the elliptical (elongated) shape of the vortex ring core. This model is hereafter referred to as the VRE (for *vortex rings with elliptical core*). The introduction of the VRE was motivated by numerical and experimental observations showing that the vorticity field of unconfined or confined vortex rings deforms with time [54]; at later stages it becomes elongated due to the Reynolds number effects [27, 31]. For confined vortex rings, this deformation is accentuated by their interaction with the lateral walls [29], leading to changes in vortex ring integral characteristics. The description of the vorticity distribution in the VRE model was based on the previous model for unconfined elliptical-core vortex rings suggested by Kaplanski *et al.* [55]:

$$\omega_{\mathrm{VRE}} = \frac{\Gamma_0}{R_0^2}\frac{\theta_e^3}{\beta\sqrt{2\pi}}\exp\left(-\frac{[r_1^2 + (x_1/\beta)^2 + 1]\theta_e^2}{2}\right)\mathrm{I}_1\left(r_1\theta_e^2\right), \tag{18}$$

where

$$\theta_e = \lambda\theta_c = \frac{R_0}{L_e}. \tag{19}$$

Compared to the quasi-isotropic Gaussian distribution (13), the vorticity distribution (18) uses two parameters, β and λ, describing the deformation (elongation or compression) along axes x and r, respectively. For the sake of simplicity, a new viscous length scale L_e was introduced in (19), with $L_e = L_c/\lambda$. Thus, we can use β and θ_e (or β and $L_e = R_0/\theta_e$) as the two parameters that fully describe the vorticity distribution in an elliptical-core vortex ring of given radius R_0. Note that the vorticity distribution (18) was derived by imposing weak perturbations on the first-order solution (13), in order to find an approximation of the non-linear solution to the Navier-Stokes equations for high Reynolds numbers. Using the vorticity function (18) within Brasseur's approach to derive the stream function correction due to the tube wall involved some technical analytical developments, presented in detail in [30]. Closed formulae were obtained for the two terms in (9). The VRE model for the confined vortex ring was finally described

by the vorticity distribution (18) and stream functions:

$$\Psi_{\text{VRE}} = (\Gamma_0 R_0)\frac{r_1 \theta_e}{4} \int_0^\infty \exp\left((\beta^2 - 1)\frac{\mu^2}{2}\right)\left[\exp(\mu x_1 \theta_e)\operatorname{erfc}\left(\frac{\mu\beta + x_1\theta_e/\beta}{\sqrt{2}}\right)\right.$$

$$\left. + \exp(-\mu x_1 \theta_e)\operatorname{erfc}\left(\frac{\mu\beta - x_1\theta_e/\beta}{\sqrt{2}}\right)\right] \mathrm{J}_1\left(\theta_e\mu\right)\mathrm{J}_1\left(r_1\theta_e\mu\right)d\mu, \tag{20}$$

and

$$\Psi_{\text{VRE}}^0 = (\Gamma_0 R_0)\frac{r_1}{\pi}\int_0^\infty \exp\left(-(\beta^2 - 1)\frac{\mu^2}{2\theta_e^2}\right)\frac{\mathrm{K}_1(\mu/\varepsilon)}{\mathrm{I}_1(\mu/\varepsilon)}\mathrm{I}_1(r_1\mu)\mathrm{I}_1(\mu)\cos(\mu x_1)d\mu. \tag{21}$$

The VRE model will be used in the following to describe confined vortex rings simulated numerically. The translational velocity predicted by the model can be inferred from the following fundamental equation (see Helmholtz [56]; Lamb [51]):

$$U_{\text{VRE}} = \int_{-\infty}^\infty \int_0^{R_w}\left(\Psi_{\text{VRE}}^w - 6x\frac{\partial\Psi_{\text{VRE}}^w}{\partial x}\right)\omega_{\text{VRE}}drdx \bigg/ \left(2\int_{-\infty}^\infty \int_0^{R_w} r^2\omega_{\text{VRE}}drdx\right). \tag{22}$$

To compare the predictions of the model with DNS data, one needs to estimate the values of parameters β and θ_e at a given time instant $\tau = \tau_f$. Using (18) for the vorticity distribution, with the approximation $I_1(r_1\theta_e^2) \approx \exp(r_1\theta_e^2)/\sqrt{2\pi r_1\theta_e^2}$, valid for large $(r_1\theta_e^2)$ (in our case, for $r_1 > 0$ and $\theta_e > 4$), we fitted the DNS vorticity field with the expression:

$$\omega_{ef} = \frac{\Gamma_{0f}}{\pi}\left(\frac{R_{0f}}{r}\right)^{1/2}\frac{1}{2\beta L_{ef}^2}\exp\left(-\frac{1}{2L_{ef}^2}(r - R_{0f})^2 - \frac{1}{2(\beta L_{ef})^2}(x - X_{0f})^2\right). \tag{23}$$

Since FreeFem++ is interfaced to the state-of-the-art optimizer Ipopt [57] using the interior point minimization method, one can compute a fully non-linear fit of all five independent parameters in (23): $\Gamma_{ef}, R_{0f}, X_{0f}, \frac{1}{2L_{ef}^2}, \frac{1}{2\beta^2 L_{ef}^2}$. A simpler alternative is to take the values for $(R_{0f}, X_{0f}, \Gamma_{ef})$ from DNS and to fit the remaining two parameters: L_{ef} and β. Here we used the second procedure, which has the advantage of being very fast and more convenient for a practical application of the model to describe experimental or numerically generated vortex rings. Also, it can be useful for the reconstruction of the velocity field generated around a vortex ring when only incomplete measurements of the velocity are available [58, 59].

An illustration of how accurately the vortex ring model can describe the geometry of the DNS vortex ring is presented in Figure 8. The values of the parameters used in the model to reconstruct vorticity and stream function fields are shown in Table III. After fitting L_{ef} and β, parameter $\theta_{ef} = R_{0f}/L_{ef}$ is computed to complete the definition of the theoretical vortex ring. Formula (18) is then used to reconstruct the theoretical vorticity field $\omega(r, x)$ and compute integral characteristics in the same way as in DNS (taking into account only the vorticity of the vortex core for which $\omega/\omega_{max} > 0.05$). Figure 8a shows that the vorticity distribution of the DNS vortex is elongated along the x-axis and can be reasonably described by an elliptical shape, as in the theoretical model. Also, one can see an asymmetric (with respect to its centre) deformation in the r-direction of the vortex predicted by DNS, which cannot be explained based on the assumption of a simple elliptic geometry.

On the other hand, Figure 8b shows that the model accurately describes the stream function distribution of the vortex ring. The deformation of the stream function near the lateral wall is correctly reproduced based on Equations (9), (20) and (21). For DNS data, streamfunction ψ is computed by solving (8) numerically with vorticity corresponding to the vortex ring core ($\omega/\omega_{max} \geq 0.05$). The vorticity layer generated at the wall is ignored, to allow comparison with the theoretical model which does not take into account such effects. Good agreement between DNS data and predictions of the model for the normalised streamfunction contours confirms the hypothesis that the stream function is not sensitive to the details of the vorticity distribution (see Danaila et $al.$ [29, 30]).

Table III shows the exact values of the parameters used to reconstruct the pinched-off vortex ring using the confined elliptical-core vortex ring model. For a typical case of confinement ratio $D_w/D = 3$, the vortex ring can be considered as detached from the trailing slug at $\tau = 14$ for the PS injection program (Figure 8) and $\tau = 12$ for the NS case. Parameters R_{0f}, X_{0f}, Γ_f are taken from the DNS simulation, while β, L_e and θ_e are computed by fitting the vorticity distribution (18) with DNS data. After truncating the theoretically reconstructed vorticity field at $\omega/\omega_{max} \geq 0.05$, as in the post-processing of DNS data, the values of the circulation Γ_{VR} and non-dimensional energy E_{VR}^* of the vortex ring are computed and compared to the corresponding values Γ_f and E^* obtained from DNS data. Note that the
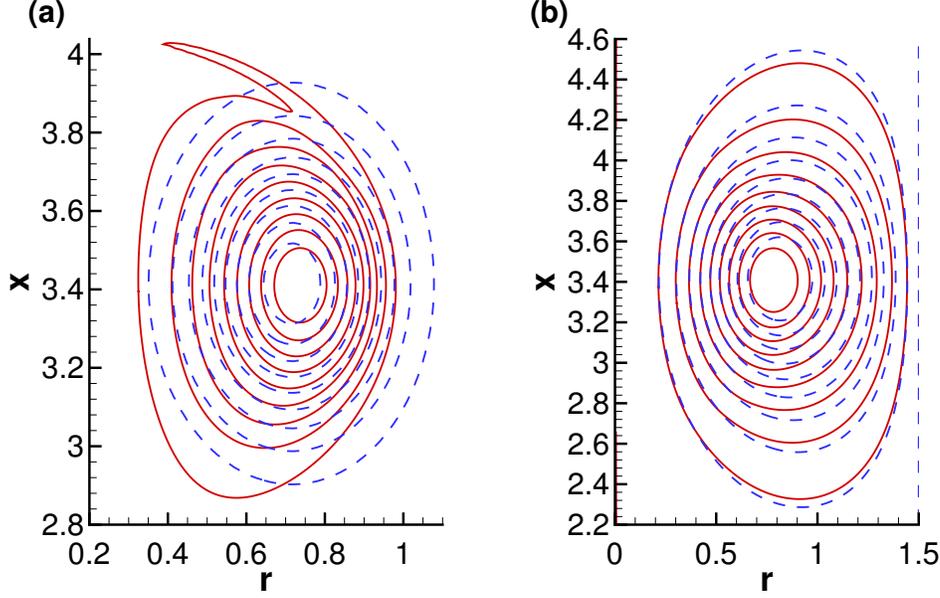
FIG. 8. Contours of normalised vorticity ω/ω_{max} (a) and corresponding normalised stream function ψ/ψ_{max} (b): DNS results (solid lines) and the prediction of the vortex ring model (dashed lines) after fitting parameters L_{ef} and β (values indicated in Table III). Values of ω/ω_{max} and ψ/ψ_{max} are shown from 0.1 to 0.9 with increments of 0.1. Case PS, $D_w/D = 3$, $\tau = 14$.

Case PS, $D_w/D = 3$, $\tau = 14$.											
Inferred from DNS data				Fitted to DNS			Computed after fit				
R_{0f}	X_{0f}	Γ_f	E^*	β	L_e	θ_e	Γ_{VR}	E^*_{VR}	b	B	$(L/D)_{\mathrm{VR}}$
0.735	3.415	1.39	0.26	1.43	0.16	4.59	1.33	0.27	0.71	0.59	3.8

Case NS, $D_w/D = 3$, $\tau = 12$.											
Inferred from DNS data				Fitted to DNS			Computed after fit				
R_{0f}	X_{0f}	Γ_f	E^*	β	L_e	θ_e	Γ_{VR}	E^*_{VR}	b	B	$(L/D)_{\mathrm{VR}}$
0.745	3.365	1.24	0.30	1.33	0.14	5.32	1.21	0.32	0.71	0.64	3.4

TABLE III. Parameters of the model describing the confined vortex ring at pinch-off.

agreement between the DNS vortex ring and the theoretically reconstructed one is very good. The reconstructed vortex ring has slightly lower circulation compared with the one inferred from DNS data ($\Gamma_{\mathrm{VR}} \lesssim \Gamma_f$), but their non-dimensional energies are similar $E^*_{\mathrm{VR}} \gtrsim E^*$.

The fit of the model parameters with DNS data was investigated for the entire post-formation phase ($\tau \geq 10$). Figure 9 (a, b) shows that the ellipticity parameter β is almost constant after pinch-off. The PS injection program generates more elongated vortex rings (higher values of β) than the NS program. Also, for confinement ratios $D_w/D \geq 4$, we approach the asymptotic limit represented by the unconfined vortex ring, with the elongation parameter $\beta \approx 1.4$ for the PS case and $\beta \approx 1.3$ for the NS case. These values are in agreement with previously published data [55]. The time evolution of the viscous parameter θ_e, given by (19), is shown in Figure 9 (c, d). For unconfined vortex rings, relevant to practical applications [18, 31], typical values of θ_e were reported to range between 3 and 4.5. The reduction of the viscous parameter θ_e with time depends on the injection program. In theoretical models, heuristic power-laws are commonly used to model the decrease of θ_e with time [53]. The exact determination of the exponent of the power-law would imply following the vortex ring post-formation evolution for a long time. For the present investigation, only the values of parameters θ_e and β at the pinch-off are relevant to the prediction of the formation time, as described in the next section.
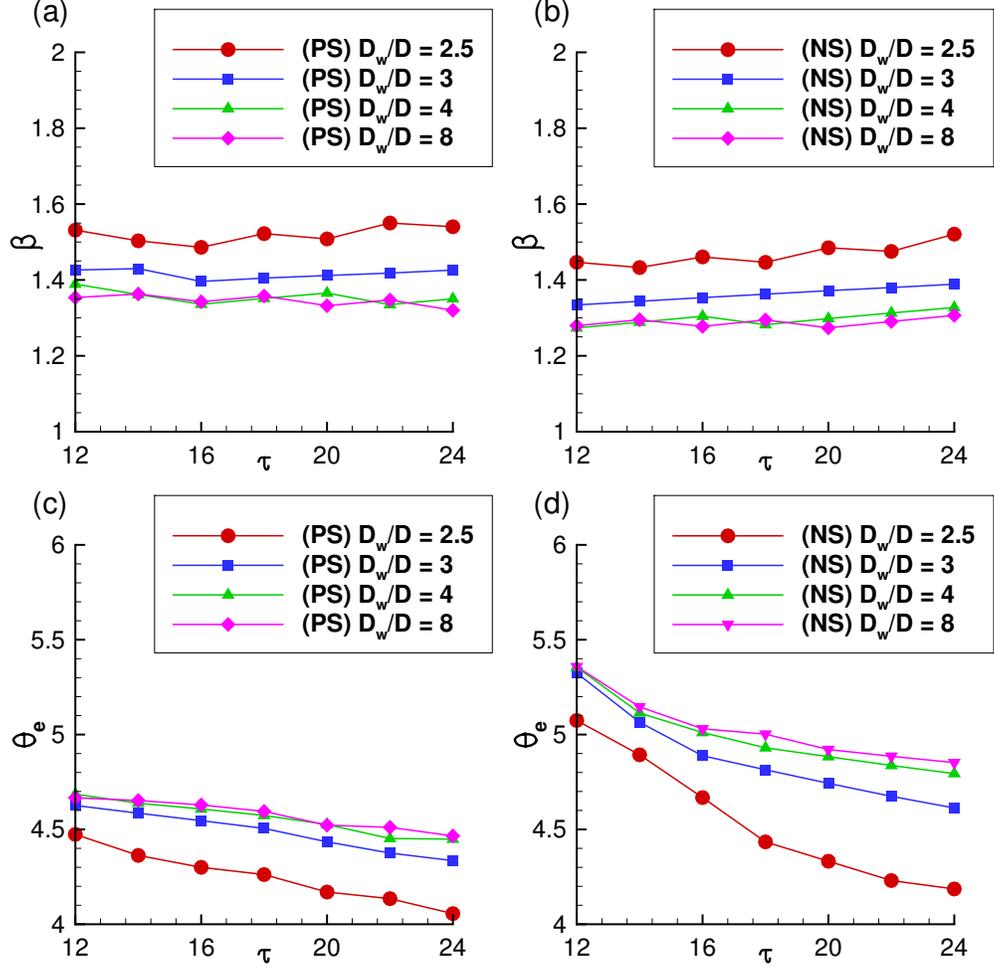
FIG. 9. Time evolution of the parameters describing the vortex ring geometry during the post-formation phase. Parameter θ_e is related to the viscous length of the model (19), while $\beta > 0$ describes the elongation along the longitudinal x-axis. All parameters are fitted from DNS data. PS (a, c) and NS (b, d) injection programs were used for the analysis.

B. Prediction of the formation number

Shusser and Gharib [21] assumed that the pinch-off starts when the translational velocity of the vortex ring equals the jet velocity near the vortex. The latter is generally predicted using the classical slug-flow model. It is possible to refine the predictions of this model by taking into account several effects in the slug-flow model, such as the boundary layer correction for the centerline velocity at the vortex generator exit [32, 60, 61], the specific form of the piston velocity program [23], or the over-pressure correction at the cylinder exit [25, 62].

In what follows, we suggest a unified frame for different versions of Shusser and Gharib's pinch-off model. Assuming that the flow rate near the vortex ring $Q_1 = (\pi R_{\mathrm{VR}}^2) U_{\mathrm{VR}}$ equals the flow rate delivered by the vortex generator $Q_2 = (\pi D^2/4) U_{\mathrm{CL}}$, the pinch-off is expected when

$$U_{\mathrm{VR}} = \frac{D^2}{4 R_{\mathrm{VR}}^2} U_{\mathrm{CL}}, \tag{24}$$

where U_{VR} is the translational velocity of the vortex ring, R_{VR} is its radius, D is the diameter of the vortex generator pipe and U_{CL} the centreline velocity of the injected flow profile at the pipe exit. The centreline velocity is time dependent and can be described as

$$U_{\mathrm{CL}}(\tau) = U_0 U_p(\tau) \chi(\tau), \tag{25}$$

where U_0 is the piston bulk velocity, U_p the piston velocity program (see Equation (4)) and χ a correction accounting for the growth of the boundary layer at the cylinder wall during the injection process. The following expression for χ was used for long-time injection programs [32]:

$$\chi(\tau) = \frac{1}{1 - \dfrac{8}{\sqrt{\pi Re_{\mathrm{D}}}}\sqrt{\tau} + \dfrac{8}{Re_{\mathrm{D}}}\tau}. \tag{26}$$

The injected flow can be described by the so-called slug-flow model [16, 17] which provides simple expressions for the circulation, impulse and energy delivered at the vortex generator (*i.e.* cylinder) exit:

$$\Gamma_s(\tau) = \frac{U_0 D}{2}\int_0^\tau \left(\frac{U_{\mathrm{CL}}(s)}{U_0}\right)^2 ds + \Gamma_p = \frac{U_0 D}{2}\left(\alpha_s(\tau) + \alpha_p\right), \tag{27}$$

$$I_s(\tau) = \frac{\pi D^3 U_0}{4}\int_0^\tau \left(\frac{U_{\mathrm{CL}}(s)}{U_0}\right)^2 ds = \frac{\pi D^3 U_0}{4}\alpha_s(\tau), \tag{28}$$

$$E_s(\tau) = \frac{\pi D^3 U_0^2}{8}\int_0^\tau \left(\frac{U_{\mathrm{CL}}(s)}{U_0}\right)^3 ds = \frac{\pi D^3 U_0^2}{8}\beta_s(\tau). \tag{29}$$

Using (25), the non-dimensional functions used in the previous expressions are presented as:

$$\alpha_s(\tau) = \int_0^\tau \left(U_p(s)\chi(s)\right)^2 ds, \quad \beta_s(\tau) = \int_0^\tau \left(U_p(s)\chi(s)\right)^3 ds. \tag{30}$$

Note the difference between this approach and that of the classical slug-flow model (5) in which the approximation $U_{\mathrm{CL}} \approx U_p$ is generally used. In Expression (27) for the slug-flow circulation, we introduced the correction [25] α_p due to the over-pressure arising at the cylinder exit plane. It is well known that the classical slug-flow model, for which $\alpha_p = 0$, underestimates the circulation injected in the flow by the vortex generator. Models for the over-pressure correction were suggested depending on the type of vortex generator (orifice or nozzle) [25] and the type of injection (parallel or with non-zero radial velocity) [63].

The piston stroke ratio is calculated as

$$\left(\frac{L}{D}\right)_s(\tau) = \int_0^\tau U_p(s)ds = \gamma_s(\tau). \tag{31}$$

It is useful to introduce the expression for the non-dimensional energy [1] inferred from the slug-flow model:

$$E_s^*(\tau) = \frac{E_s(\tau)}{\sqrt{I_s(\tau)\Gamma_s(\tau)^3}} = \sqrt{\frac{\pi}{2}}\frac{\beta_s}{\sqrt{\alpha_s\left(\alpha_s + \alpha_p\right)^3}}. \tag{32}$$

The next step in the approach suggested by Shusser and Gharib [21] is to link the predictions of the slug-flow model with the characteristics of the actual vortex ring, observed at the pinch-off. To this end, the vortex ring is usually described by a vortex ring model allowing one to express the main integrals of motion as functions of its geometric characteristics. The Norbury-Fraenkel vortex ring model [26] is largely used for this purpose [1, 7, 9, 21, 23, 61] since a single geometric parameter is necessary to express the ring's integral characteristics. However, in the Norbury-Fraenkel model the vorticity distribution in the vortex core is linear, *i.e.* proportional to the distance to the axis of symmetry (as in Hill's spherical vortex model), which is different from the quasi-Gaussian distribution observed for unconfined [27, 28] or confined vortex rings [20, 29, 30]. Therefore, a more realistic vortex ring model, described in the preceding section, will be used for this part of the pinch-off model.

The vortex ring can be described using the following non-dimensional parameters [21, 22, 60]:

$$b = R_{\mathrm{VR}}\sqrt{\frac{\pi \Gamma_{\mathrm{VR}}}{2 I_{\mathrm{VR}}}}, \quad B = U_{\mathrm{VR}}\sqrt{\frac{\pi I_{\mathrm{VR}}}{\Gamma_{\mathrm{VR}}^3}}. \tag{33}$$

Using the pinch-off criterion (24) and further assuming that at the pinch-off $\Gamma_{\mathrm{VR}} \approx \Gamma_s$ and $I_{\mathrm{VR}} \approx I_s$ we can derive the following equation:

$$\frac{\pi\sqrt{2}}{4}\frac{1}{b^2 B} = \frac{\sqrt{\alpha_s(\tau)(\alpha_s(\tau) + \alpha_p)}}{U_p(\tau)\chi(\tau)}, \tag{34}$$

which has to be solved once the left-hand side is estimated from the vortex ring parameters at pinch-off. The solution gives us the formation time τ_f and the formation number:

$$F = \left(\frac{L}{D}\right)_f = \gamma_s(\tau_f). \tag{35}$$

The link between this approach and the previous formulations of the pinch-off model by Shusser and Gharib can be obtained by introducing

$$\left(\frac{L}{D}\right)_{\text{VR}} = \frac{\pi\sqrt{2}}{4}\frac{1}{b^2 B}, \tag{36}$$

which is the expression of the formation number obtained if a classical slug-flow model, with constant piston velocity ($U_p(\tau) = 1$) and no corrections ($\chi(\tau) = 1$, $\alpha_p = 0$), is considered. Indeed, for this case, we obtain from (30) that $\alpha_s = \beta_s = \gamma_s = \tau$ and finally from (34) and (36) that $(L/D)_{\text{VR}} = \tau$. The formation number for this case is inferred directly from (35) as $(L/D)_f = \tau_f = (L/D)_{\text{VR}} = \frac{\pi\sqrt{2}}{4}\frac{1}{b^2 B}$. The corresponding non-dimensional energy is obtained from Equation (32) as $E_f^* = \sqrt{\frac{\pi}{2}}\frac{1}{\tau_f}$. These formulae were extensively used in the literature to predict the value of the formation number [1, 7, 9, 21, 22, 31] or the value of the translational velocity of the vortex ring [5].

Corrections taking into account the boundary-layer growth at the wall of the cylinder were used by considering [32, 60, 61] $U_p(\tau) = 1$ and different formulae for $\chi(\tau)$ (e. g. Equation (26)). The influence of the piston velocity program was assessed [23] by taking $\chi(\tau) = 1$ and different $U_p(\tau)$ (impulsive, linear, and trapezoidal velocity programs).

For the present study, we consider the piston velocity program $U_p(\tau)$ expressed by (4) and ignore the boundary-layer correction (i. e. $\chi = 1$), since injection times are short. On the other hand, we use the over-pressure correction model [25] suggesting that for the orifice vortex generator (used in our simulations) $\Gamma_p \approx \frac{U_0 D}{2}$ and hence $\alpha_p \approx 1$. The vortex ring at pinch-off is described by the model suggested by Danaila *et al.* [30] for confined viscous vortex rings with elliptical cores. We use the fitted parameters from Table III to compute the values for b, B and $(L/D)_{\text{VR}}$ from (33). These computed values are shown in the last three columns of Table III.

Note that parameter $(L/D)_{\text{VR}}$ depends on the geometric characteristics of the vortex ring: the ellipticity parameter β and the ratio θ_e between the vortex radius and its viscous characteristic length (cf. Equations (18) and (19)). Figure 10 illustrates this dependency. The values for the PS and NS simulations presented in Table III are shown as circle and square, respectively. Figure 10 covers a large range of values of β and θ_e, typical for numerically or experimentally generated vortex rings.
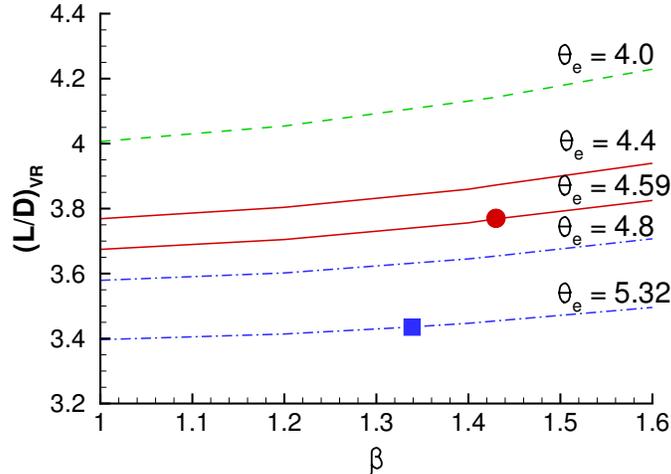

FIG. 10. The values of $(L/D)_{\text{VR}}$ (see Equation (36)) versus geometrical parameters β and θ_e (cf. Equations (18) and (19)). The symbols show the values taken from Table III for the PS (circle) and NS (square) injection programs.

Finally, we used the values taken from Table III to solve Equation (34) and find the value of the formation time τ_f, and the formation number from Equation (35). We obtained $\tau_f = 6.2$ ($F = 3.39$) for the PS program and $\tau_f = 4.1$ ($F = 2.76$) for the NS program. These values are close to the DNS values from Table II: $F = 3.22$ and $F = 2.51$ for the PS and NS programs, respectively.

IV. SUMMARY

The results of a number of numerical experiments that investigate the properties of confined vortex rings were presented. These experiments were motivated by laboratory piston-cylinder experiments of unconfined [2] or confined [20] vortex rings. The simulated piston velocity programs match these experiments and consider triangular pulses [20] dominated by either positive (PS) or negative (NS) acceleration ramps [2].

For low confinement ratios ($D_w/D \leq 2$), the shear layer at the lateral wall rolls-up into a strong vortex and the pinch-off is not observed. The pinch-off is clearly observed for confinement ratios $D_w/D \geq 2.5$, for which the lateral shear layer is still present but its influence on the evolution of the vortex ring is reduced. For $D_w/D \geq 4$, the evolution of the confined vortex ring is similar to that of the unconfined one.

The value of the formation time τ_F, defined as the time at which the piston motion generates the amount of vorticity engulfed by the pinched-off vortex ring, was obtained. The formation number was computed as the corresponding piston stroke ratio (L/D) at the formation time. These concepts of formation time and formation number were introduced by Krueger and Gharib [2] in connection with the non-uniform (impulsive) velocity programs used for piston motion. The obtained values for the formation number ($F = 3.22$ to 3.31 for the PS and $F = 2.51$ to 2.60 for the NS injection programs) are lower than those reported for the unconfined vortex rings [2] ($F = 3.3 - 4.4$ for the PS case and $F = 2.4 - 2.9$ for the NS case). Confinement was shown to have little influence on the value of the formation time for $D_w/D \geq 3$.

Using the model suggested by Danaila *et al.* [30], the pinch-off was described by capturing the elliptical shape of the vorticity distribution in the core and the bending of the streamlines of flow near the lateral wall. These could not be captured by the Norbury-Fraenkel inviscid vortex ring model. The approach suggested by Shusser and Gharib [21] was used to predict the value of the formation number. Good predictions were obtained for both PS and NS cases.

It was suggested that the concepts of formation time and number can allow one to generate optimal confined vortex rings in a wide range of applications with confining walls, ranging from cardiac flows [4], to propulsion devices [7, 8] and internal combustion engines [19], and thus increase their efficiency.

ACKNOWLEDGMENTS

---

[1] M. Gharib, E. Rambod, and K. Shariff, "A universal time scale for vortex ring formation," J. Fluid Mech. **360**, 121–140 (1998).

[2] S. Krueger and M. Gharib, "The significance of vortex ring formation on the impulse and thrust of a starting jet," Phys. Fluids **15**, 1271 (2003).

[3] K. Mohseni, "Statistical equilibrium theory for axisymmetric flow: Kelvin's variational principle and an explanation for the vortex ring pinch–off process," Phys. Fluids **13**, 1924 (2001a).

[4] M. Gharib, E. Rambod, A. Kheradvar, D. J. Sahn, and J. O. Dabiri, "Optimal vortex formation as an index of cardiac health," Proceedings of the National Academy of Sciences (PNAS) **103**, 6305–6308 (2006).

[5] K. Mohseni, "A formulation for calculating the translational velocity of a vortex ring or pair," Bioinspiration & Biomimetics **1**, S57–S64 (2006).

[6] J. O. Dabiri, "Optimal vortex formation as a unifying principle in biological propulsion," Annual Review of Fluid Mechanics **41**, 17–33 (2009).

[7] P. F. Linden and J. S. Turner, "The formation of 'optimal' vortex rings, and the efficiency of propulsion devices," J. Fluid Mech. **427**, 61 (2001).

[8] J. M. Lawson and J. R. Dawson, "The formation of turbulent vortex rings by synthetic jets," Phys. Fluids **25**, 105113 (2013).

[9] M. Rosenfeld, E. Rambod, and M. Gharib, "Circulation and formation number of a laminar vortex ring," J. Fluid Mech. **376**, 297–318 (1998).

[10] J. O. Dabiri and M. Gharib, "Starting flow through nozzles with temporally variable exit diameter," J. Fluid Mech. **538**, 111–136 (2005).

[11] S. Krueger, J. O. Dabiri, and M. Gharib, "Vortex ring pinch–off in the presence of simultaneously initiated uniform background co–flow," Phys. Fluids **15**, L49 (2003).

[12] J. O. Dabiri and M. Gharib, "Delay of vortex ring pinchoff by an imposed bulk conterflow," Phys. Fluids **16**, L28 (2004).

[13] K. Schlueter-Kuck and J. O. Dabiri, "Pressure evolution in the shear layer of forming vortex rings," Phys. Rev. Fluids **1**, 012501 (2016).

[14] M. Shusser and M. Gharib, "A model for vortex ring formation in a starting buoyant plume," J. Fluid Mech. **416**, 173–185 (2000).

[15] R. Q. Wang, A. W. K. Law, and E. E. Adams, "Pinch-off and formation number of negatively buoyant jets," Phys. Fluids **23**, 052101 (2011).

[16] K. Shariff and A. Leonard, "Vortex rings," Ann. Rev. Fluid Mech. **24**, 235–279 (1992).

[17] T. T. Lim and T. B. Nickels, "Vortex rings," in Fluid Vortices, edited by S. I. Green (Kluwer, 1995) p. 95.

[18] Y. Fukumoto, "Global evolution of viscous vortex rings," Theor. Comput. Fluid Dynamics **24**, 335–347 (2010).

[19] S. Begg, F. Kaplanski, S. S. Sazhin, M. Hindle, and M. Heikal, "Vortex ring-like structures in gasoline fuel sprays under cold-start conditions," International Journal of Engine Research **10**, 195–214 (2009).

[20] K. Stewart, C. Niebel, S. Jung, and P. Vlachos, "The decay of confined vortex rings," Experiments in Fluids **53**, 163–171 (2012).

[21] M. Shusser and M. Gharib, "Energy and velocity of a forming vortex ring," Phys. Fluids **12**, 618 (2000).

[22] K. Mohseni and M. Gharib, "A model for universal time scale of vortex ring formation," Phys. Fluids **10**, 2436–2438 (1998).

[23] M. Shusser, M. Rosenfeld, J. O. Dabiri, and M. Gharib, "Effect of time–dependent piston velocity program on vortex ring formation in a piston/cylinder arrangement," Phys. Fluids **12**, 033601 (2006).

[24] L. Gao and S. C. M. Yu, "A model for the pinch-off process of the leading vortex ring in a starting jet," J. Fluid Mech. **656**, 205–222 (2010).

[25] P. S. Krueger and M. Gharib, "An over–pressure correction to the slug model for vortex ring calculation," J. Fluid Mech. **545**, 427–443 (2005).

[26] J. Norbury, "A family of steady vortex rings," J. Fluid Mech. **57**, 417–431 (1973).

[27] A. Weigand and M. Gharib, "On the evolution of laminar vortex rings," Exp. Fluids **22**, 447–457 (1997).

[28] J. E. Cater, J. Soria, and T. T. Lim, "The interaction of the piston vortex with a piston-generated vortex ring," J. Fluid Mech. **499**, 327–343 (2004).

[29] I. Danaila, F. Kaplanski, and S. Sazhin, "Modelling of confined vortex rings," J. Fluid Mech. **774**, 267–297 (2015).

[30] I. Danaila, F. Kaplanski, and S. Sazhin, "A model for confined vortex rings with elliptical core vorticity distribution," J. Fluid Mech. **811**, 67–94 (2017).

[31] I. Danaila and J. Helie, "Numerical simulation of the postformation evolution of a laminar vortex ring," Phys. Fluids **20**, 073602 (2008).

[32] I. Danaila, C. Vadean, and S. Danaila, "Specified discharge velocity models for the numerical simulation of laminar vortex rings," Theor. Comput. Fluid Dynamics **23**, 317–332 (2009).

[33] M. Rai and P. Moin, "Direct simulations of turbulent flow using finite–difference schemes," J. Comput. Physics **96**, 15–53 (1991).

[34] R. Verzicco and P. Orlandi, "A finite–difference scheme for three–dimensional incompressible flow in cylindrical coordinates," J. Comput. Physics **123**, 402–414 (1996).

[35] P. Orlandi, *Fluid Flow Phenomena: A Numerical Toolkit* (Kluwer Academic Publishers, Dordrecht, 1999).

[36] M. R. Ruith, P. Chen, and E. Meiburg, "Development of boundary conditions for direct numerical simulations of three–dimensional vortex breakdown phenomena in semi–infinite domains," Computers & Fluids **33**, 1225–1250 (2004).

[37] J. Kim and P. Moin, "Application of a fractional step method to incompressible Navier–Stokes equations," J. Comput. Physics **59**, 308–323 (1985).

[38] W. Zhao, H. F. Steven, and L. G. Mongeau, "Effects of trailing jet instability on vortex ring formation," Phys. Fluids **12**, 589–596 (2000).

[39] A. Michalke, "Survey on jet instability theory," Prog. Aerospace Sci. **21**, 159–199 (1984).

[40] S. James and C. K. Madnia, "Direct numerical simulation of a laminar vortex ring," Phys. Fluids **8**, 2400–2414 (1996).

[41] I. Orlanski, "A simple boundary condition for unbounded hyperbolic flows," J. Comput. Physics **21**, 251–269 (1976).

[42] F. Hecht, O. Pironneau, A. Le Hyaric, and K. Ohtsuke, *FreeFem++ (manual)* (www.freefem.org, 2007).

[43] F. Hecht, "New developments in Freefem++," Journal of Numerical Mathematics **20**, 251–266 (2012).

[44] R. Sau and K. Mahesh, "Passive scalar mixing in vortex rings," J. Fluid Mech. **582**, 449–461 (2007).

[45] J. O. Dabiri and M. Gharib, "Fluid entrainment by isolated vortex rings," J. Fluid Mech. **511**, 311–331 (2004).

[46] K. Mohseni, H. Ran, and T. Colonius, "Numerical experiments on vortex ring formation," J. Fluid Mech. **430**, 267–282 (2001b).

[47] F. B. Kaplanski and Y. A. Rudi, "A model for the formation of "optimal" vortex ring taking into account viscosity," Phys. Fluids **17**, 087101–087107 (2005).

[48] Y. Fukumoto and F. B. Kaplanski, "Global time evolution of an axisymmetric vortex ring at low Reynolds numbers," Phys. Fluids **20**, 053103 (2008).

[49] J. G. Brasseur, *Kinematics and dynamics of vortex rings in a tube*, Ph.D. Thesis, report JIAA, TR-26, Joint Institute for Aeronautics and Acoustics, Dept. of Aeronautics and Astronautics, Stanford University (1979).

[50] J. G. Brasseur, "Evolution characteristics of vortex rings over a wide range of Reynolds numbers," AIAA Paper, 1986-1097:1–11 (1986).

[51] H. Lamb, *Hydrodynamics* (Dover, New York, 1932).

[52] F. B. Kaplanski and Y. A. Rudi, "Dynamics of a viscous vortex ring," Int. J. Fluid Mech. Res. **26**, 618–630 (1999).

[53] F. Kaplanski, S. S. Sazhin, Y. Fukumoto, S. Begg, and M. Heikal, "A generalized vortex ring model," J. Fluid Mech. **622**, 233–258 (2009).

[54] Y. Fukumoto and H. K. Moffatt, "Motion and expansion of a viscous vortex ring. Part 1. A higher-order asymptotic formula for the velocity." J. Fluid Mech. **417**, 1–45 (2000).

[55] F. B. Kaplanski, Y. Fukumoto, and Y. A. Rudi, "Reynolds-number effect on vortex ring evolution in a viscous fluid," Phys. Fluids **24**, 033101 (2012).

[56] H. Helmholtz, "On integrals of the hydrodynamical equations, which express vortex-motion," Phil. Mag. (ser. 4) **33**, 485–510 (1867).

[57] A. Wächter, *An Interior Point Algorithm for Large-Scale Nonlinear Optimization with Applications in Process Engineering*, Ph.D. Thesis, Carnegie Mellon University, Pittsburgh, PA, USA (2002).

[58] Y. Zhang and I. Danaila, "A finite element BFGS algorithm for the reconstruction of the flow field generated by vortex rings," Journal of Numerical Mathematics **20**, 325–340 (2012).

[59] I. Danaila and B. Protas, "Optimal reconstruction of inviscid vortices," Proceedings of the Royal Society A: Mathematical, Physical & Engineering Sciences **471**, 20150323 (2015).

[60] M. Shusser, M. Gharib, M. Rosenfeld, and K. Mohseni, "On the effect of pipe boundary layer growth on the formation of a laminar vortex ring generated by a piston-cylinder arrangement," Theor. Comput. Fluid Dynamics **15**, 303–316 (2002).

[61] J. O. Dabiri and M. Gharib, "A revised slug model boundary layer correction for starting jet vorticity flux," Theor. Comput. Fluid Dynamics **17**, 293–295 (2004).

[62] P. S. Krueger, "Circulation and trajectories of vortex rings formed from tube and orifice openings," Physica D **237**, 2218–2222 (2008).

[63] M. Krieg and K. Mohseni, "Modelling circulation, impulse and kinetic energy of starting jets with non-zero radial velocity," J. Fluid Mech. **719**, 488–526 (2013).